Applied Nanoscience (2018) 8:1587–1596
https://doi.org/10.1007/s13204-018-0835-4

ORIGINAL ARTICLE

Decoration of mesoporous graphite-like C_3N_4 nanosheets by NiS nanoparticle-driven visible light for hydrogen evolution

Mohammad W. Kadi[1] · Reda M. Mohamed[1,2] · Adel. A. Ismail[2,3] · Delft. W. Bahnemann[3,4]

Received: 24 May 2018 / Accepted: 25 June 2018 / Published online: 3 July 2018

Abstract

Separation of photogenerated electrons from holes is an important factor that increases hydrogen evolution rate in the water splitting reaction. This recombination prevention can be achieved by co-catalyst's deposition onto the semiconductor material's surfaces. In this contribution, synthesis of mesoporous C_3N_4 of graphite-like structure by a combustion technique employing high mesoporous silica as a template has been achieved. Subsequently, NiS nanoparticles were decorated as g-C_3N_4 nanosheets at various NiS contents (5–20%). the photocatalytic efficiency of the prepared NiS/g-C_3N_4 nanocomposites was investigated and compared with those of pure NiS and g-C_3N_4 for evolution of hydrogen using glycerol as a scavenger upon visible light illumination. The findings indicated that the content of deposited NiS nanoparticles onto g-C_3N_4 is significant in the enhancement of the photocatalytic response of g-C_3N_4. 15% NiS/g-C_3N_4 nanocomposite is the optimized photocatalyst and its photocatalytic activity is larger than both NiS and g-C_3N_4 by about 48 and 114 times, respectively. 15% NiS/g-C_3N_4 nanocomposite has photocatalytic stability up to five times. The enrichment of the photocatalytic efficiency of NiS/g-C_3N_4 photocatalyst could be attributed to the presence of NiS nanoparticles as co-catalyst, which enables efficient charge carrier separation of g-C_3N_4, mesostructure, large surface area and narrow band gap.

Keywords Mesoporous graphite-like C_3N_4 · NiS · Visible light · Hydrogen production

Introduction

The growing energy demand prompted scientists to explore venues of producing fuels from chemical transformations instead of depending on the limited supplies found in nature. A widely explored reaction in this regard is the hydrogen production by splitting of water with and without scavengers. The ample presence of water brings an appeal to this reaction; however, thermodynamic restrictions motivated people to look for ways to overcome those restrictions. A widely followed principle to overcome the nonspontaneity barrier (237 kJ/mol) is to employ a catalyst capable of harvesting the natural energy of the sun. This principle can also be exploited in many chemical reactions (Ismail and Bahnemann 2014; Ye et al. 2015). Most metal and nonmetal oxides require substrates and band gap tuning to achieve activity in the visible wavelength regime. Then there are questions of stability and environmental suitability (Li et al. 2015; Chen et al. 2012). Graphitic carbon nitrides (g-C_3N_4) are class of materials that show promising applications. This is because of their covalent bonding structure which brings about stability and the medium band gap structure that allows application in the visible spectrum range. The ability to easily dope and incorporate metal oxides and other compounds or atoms within the structure of g-C_3N_4 opens up possibilities of large improvements in the catalytic efficiency of the material. Several approaches were explored to synthesize the g-C_3N_4 nanosheets with and without incorporation of other materials (Dong et al. 2014; Ganesh Babu et al. 2015; Raza et al. 2017; Mozaffari et al. 2017a, b; Prakash et al. 2018;

✉ Reda M. Mohamed
redama123@yahoo.com

1 Department of Chemistry, Faculty of Science, King Abdulaziz University, P.O. Box 80203, Jeddah 21589, Kingdom of Saudi Arabia

2 Advanced Materials Department, Central Metallurgical R&D Institute, CMRDI, P.O. Box 87, Helwan, Cairo 11421, Egypt

3 Photocatalysis and Nanotechnology Unit, Institute of Technical Chemistry, Leibniz Hannover University, Callinstr. 3, 30167 Hannover, Germany

4 Photoactive Nanocomposite Materials, Saint-Petersburg, State University, Ulyanovskaya Str, Peterhof, Saint-Petersburg 198504, Russia

Misra et al. 2015, 2017; Singh et al. 2017, 2016; Tyagi et al. 2016; Du et al. 2018; Lin et al. 2017; Mai et al. 2017; Jin et al. 2014; Bao and; Chen 2017; Liu et al. 2015; Peng et al. 2014). The use of g-C_3N_4 in catalytic reactions has been widely explored, for example, liberation of 842 µmol/h/g H_2 from splitting of water was achieved upon illumination under visible light using crumpled Cu_2O-g-C_3N_4 nanosheets (Anandan et al. 2017). In another example, a significant improvement in H_2 production was achieved by incorporating TiO into the C_3N_4 nanosheets (Hafeez et al. 2018).

Nickel sulfide (NiS) is an interesting material that has been used in different potential applications such as catalysis and photocatalysis, electrodes and capacitors and solar cells (Kristl et al. 2017; Luo et al. 2017, 2018; Yang et al. 2018; Liua et al. 2018; Wen et al. 2017). Its favorable properties prompted researchers to incorporate its various forms into g-C_3N_4 nanosheets. Wen et al. examined the incorporation of g-C_3N_4, carbon black and NiS in amorphous phase to form composite g-C_3N_4 nanosheet-carbon black-NiS photocatalyst. The produced hydrogen production rate was found to be 992 µmol/g/h upon illumination under visible light in the reaction of water splitting (Wen et al. 2015). The approximate hydrogen evolution rate of 16,400 µmol/g/h was received using loading percent 0.76 wt% of NiS onto g-C_3N_4 (Zhao et al. 2018). Urea pyrolysis and ion exchange procedures were employed to produce an efficient g-carbon nitride/NiS photocatalyst for hydrogen evolution (Chen et al. 2014). A one-pot preparation of NiS/g-C_3N_4 heterojunction was obtained and evaluated for water splitting and it exhibited 29.68 µmol/g/h of H_2 production rate (Hea et al. 2018). In this contribution, decoration of mesoporous graphite-like C_3N_4 nanosheets by NiS nanoparticles at varied contents (5–20%) have been developed for hydrogen production using glycerol as a scavenger upon visible light illumination. The findings indicated that 15% NiS/g-C_3N_4 is the optimized photocatalyst and its photocatalytic activity is greater than both pure g-C_3N_4 and NiS by about 114 and 48 times, respectively.

Experimental

Synthesis of NiS nanoparticles/mesoporous g-C_3N_4

Dicyandiamide and urea were purchased from Sigma-Aldrich. In an effort to achieve high surface area g-C_3N_4, mesoporous silica (HMS) with large surface area (ca. 500–1000 m^2/g) and the pyrolysis of urea and dicyandiamide in air was employed. Detailed procedure of the HMS production can be found elsewhere (Mohamed and Aazam 2011). 1 g of HMS was added in distilled water (50 mL) with 30 min sonication. 5 g urea and 3 g of dicyandiamide were gradually added to the above solution with continuous agitation at a temperature of 80 °C until completely dissolved. Excess water was removed by drying at 80 °C over night. This was followed by 4 h calcination at 550 °C. Finally, the product was immersed in 2 M NH_4HF_2 solution (50 mL) with vigorous stirring for 24 h to eliminate the hard HMS template. The delivered material was washed and cleaned many times using water to get rid of any adsorbed contaminants onto the surface of the synthesized g-C_3N_4 photocatalyst; afterward the pure and cleaned g-C_3N_4 was subjected to drying at about 100 °C for 12 h. On the other hand, NiS nanoparticles were fabricated using a hydrothermal process in which 0.16 g of nickel nitrate hexahydrate and 0.12 g of thiourea were added and dissolved in 30 mL distilled water. The mixture was agitated for 0.5 h and the resultant colloidal suspension was removed and kept in a Teflon-lined autoclave at 200 °C for 10 h. The produced precipitate was gathered and cleaned several times using distilled water and kept overnight in a drier at 110 °C. The decoration of mesoporous g-C_3N_4 nanosheet by NiS nanoparticles was prepared using a hydrothermal method, which involved 30 min sonication of synthesized g-C_3N_4 in 30 mL of distilled water followed by addition of 0.16 g of nickel nitrate hexahydrate and 0.12 g of thiourea to the aqueous solution slowly with agitation for 1 h. The mixture then was kept in Teflon-lined autoclave at 200 °C for 10 h. The produced precipitate was gathered and washed several times using ethanol and distilled water and dried under vacuum for 12 h at 80 °C. Many series of NiS/g-C_3N_4 nanocomposites having various NiS wt% were prepared and designated the label X wt% NiS/g-C_3N_4, where X is the weight percentage of NiS.

Characterization

Morphology and microstructure were investigated via JEOL-JEM-1230 transmission electron microscope (TEM). A Chromatech apparatus of Nova 2000 series was utilized investigate the texture properties of the prepared specimens by applying N_2-adsorption measurements. Bruker axis D8 XRD instrument was used to determine the crystalline phase. A Shimadzu RF-5301 fluorescence spectrophotometer was used to record photoluminescence emission spectra (PL). Band gap values were derived from UV–visible diffuse reflectance spectra using UV–Vis–NIR spectrophotometer (V-570, Jasco, Japan).Transient photocurrent measurements were conducted by deposition of the prepared samples onto conducting glass Indium–tin–oxide slices (ITO) (1.0 × 1.0 cm) that were chemically cleaned in various steps. Zahner Zennium's electrochemical workstation was employed to record the photocurrent intensity.

Photocatalytic tests

In the hydrogen evolution reaction, a known weight of the photocatalyst was dispersed into 450 mL 10% vol glycerol as a scavenger/H_2O. The photoreaction system was sealed and the experiments were performed at atmospheric pressure and room temperature. A quartz-jacketed cooler was used to prevent the lamp heat from affecting the reaction. After 15 min sonicated dispersion, the slurry was N_2 aerated for 30 min. The reaction mixture was illuminated by visible light-generated 500 W Xenon lamp. The produced hydrogen was investigated via gas chromatography system (Agilent GC 7890A) using N_2 gas as carrier. Illumination in the absence of the photocatalyst and a reaction without illumination were carried out to ensure that the reaction does not go forward without these conditions.

Results and discussion

Material's investigations

Figure 1 exhibits XRD diffractograms of the synthesized NiS/g-C_3N_4, NiS, g-C_3N_4 nanocomposites. The diffraction peak at 27.4° confirms the existence of g-carbon nitride sheets (JCPDS 87-1526), the pattern also reveals that the addition of NiS decreases the peak intensity of the g-C_3N_4 sheet. Diffraction peaks for NiS (JCPDS 77-1624) appear for 10, 15, and 20 wt% of the added NiS, but not at 5 wt%. This could be referred to the low NiS content and/or the good NiS dispersion onto the g-C_3N_4 surface. No ambiguous peaks in the XRD patterns were noticed proving that NiS and g-C_3N_4 sheets form a heterojunction nanocomposite.

The FTIR spectra of NiS/g-C_3N_4 nanocomposites, pure NiS and g-C_3N_4, are depicted in Fig. 2. The peak was assigned at 808/cm for NiS/g-C_3N_4 nanosheets and pure g-C_3N_4 as a result of the feature triazine units stretching mode. Also, there were five absorption peaks at 1243, 1322, 1408, 1581 and 1633/cm. They are referred to the typical CN-heterocyclic stretching mode (Kumar et al. 2013; Zhang et al. 2012). The spectra also show that the peak intensity of pure pg-C_3N_4 reduces with the boost of NiS content. Pure NiS was assigned at absorption peak at about 664/cm and it appears that the broad peak of pure NiS declined with increasing g-C_3N_4 contents which exhibited that the NiS/g-C_3N_4 nanosheets were formed.

Figure 3 illustrates the XRS spectra for the 15% NiS/g-C_3N_4 nanocomposite. The wide XPS survey scan spectrum of 15% NiS/g-C_3N_4 nanocomposite confirms the presence of Ni, S, C, and N and in the sample as shown in Fig. 3a. The high-resolution spectra for Ni, S, C, and N are depicted in Fig. 3b–e. The two main peaks were assigned at Ni 2p3/2–853.1 eV and Ni 2p1/2–860.3 (Fig. 3b); this could be explained by existing Ni^{2+} ions in the prepared nanocomposites. It is worth mentioning that these are smaller than previously mentioned values of 856.2 and 862.1 eV (Cheng et al. 2017; Chen et al. 2015), which confirm the interaction between NiS and g-C_3N_4. Figure 3c exhibited two peaks at S 2p3/2 and S 2p1/2 peaks detected at 162.2 and 163.4 eV, respectively, confirming the existence of sulfur species in the sample (Meng et al. 2013). These peaks look broad indicating the correlation between NiS and g-C_3N_4. Figure 3d displayed two main peaks at C_{1S} ~ 287.9 and C_{1S} ~ 284.6 eV, revealing the existence of sp2 C connected to N in the N-consisting aromatic rings and sp2 C–C bonds (Wang et al. 2016; Khan et al. 2018).

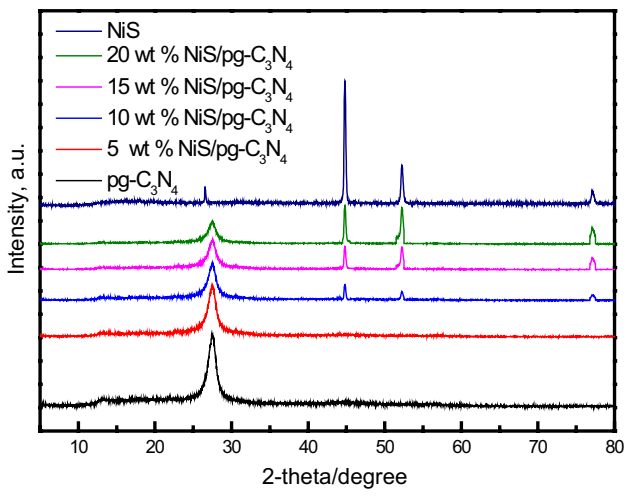

Fig. 1 XRD patterns of NiS, pg-C_3N_4, and NiS/pg-C_3N_4 nanocomposites

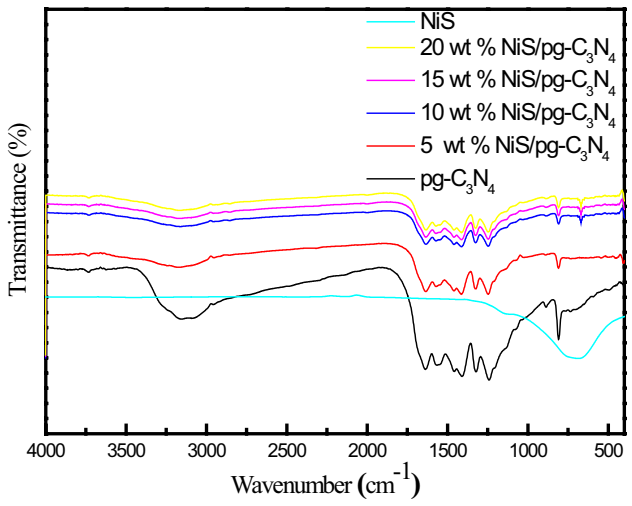

Fig. 2 FTIR spectra of pure NiS, pg-C_3N_4, and NiS/pg-C_3N_4 nanocomposites

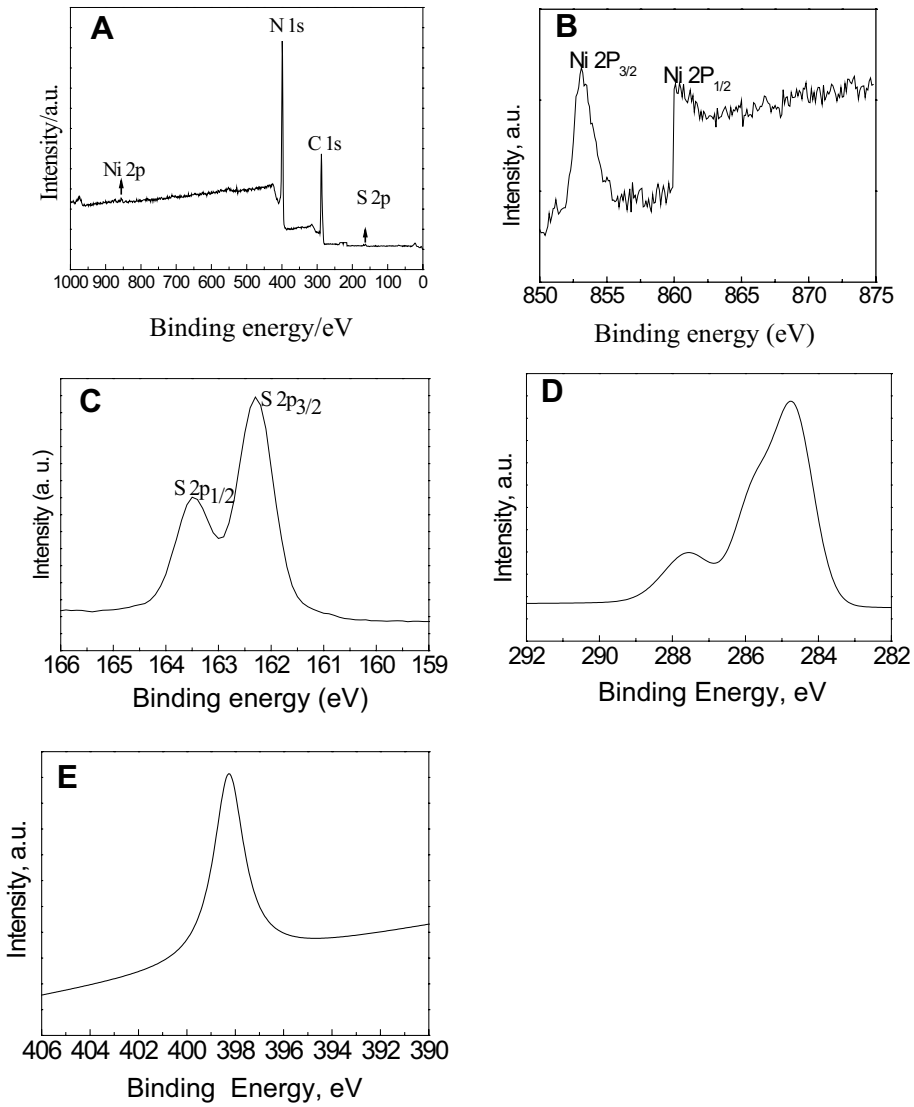

Fig. 3 XRS spectra for 15 wt% NiS/pg-C_3N_4 nanocomposite, where **a** XPS survey scan spectrum of 15 wt% NiS/pg-C_3N_4 nanocomposite, **b** high-resolution XPS spectra of Ni_{2p}, **c** high-resolution XPS spectra of S_{2p}, **d** high-resolution XPS spectra of C_{1s}, and **e** high-resolution XPS spectra of N_{1s}

N_{1S} peaks appear at 398.3 eV as shown in Fig. 3 E, confirming sp2-hybridized of the N atom. All these evidences confirm the composition of the graphitic carbon nitride (Hou et al. 2014).

Figure 4 exhibits TEM images of pure NiS nanoparticles and 15% NiS/g-C_3N_4 nanocomposite. TEM image in Fig. 4a reveals NiS nanoparticle structure with particle size in range of 25–40 nm. Figure 4b exhibits g-C_3N_4 sheet structure. Figure 4c shows the TEM image of 15% NiS/g-C_3N_4 sample; NiS particles are highly dispersed onto g-C_3N_4 sheet and decorated with spherical shape about 10 nm. Figure 5 shows HRTEM image for NiS@ pg-C_3N_4 nanocomposite sample. The results reveal that NiS is high dispersed on surface of pg-C_3N_4. The presence of lattice spacing of 0.201 nm and 0.321 nm for (102) plane and for (002) plane, respectively, confirms the presence of NiS and pg-C_3N_4, respectively. Therefore, HRTEM reveals an intimate interface between pg-C_3N_4 and NiS.

Figure 6 illustrates the N_2 adsorption–desorption isotherm of pure NiS, g-C_3N_4 and 15% NiS/pg-C_3N_4. According to IUPAC classification these correspond to isotherm types II, IV and IV, respectively, which confirms that mesoporous characteristics of g-C_3N_4 remain unchanged even after deposition of NiS on its surface (Fig. 5b, c). The surface areas of pure NiS nanoparticles, g-C_3N_4 and NiS/g-C_3N_4 nanocomposites are summarized in Table 1. The obtained results indicated that the specific area of pure g-C_3N_4 (120 m^2/g) prepared by procedures in this paper is significantly higher than values reported earlier (Chen et al. 2017). A major reason for the surface area enhancement could be the use of HMS as starting material as reported in the "Experimental" section.

The UV–Vis spectra of pure NiS, g-C_3N_4, and NiS/g-C_3N_4 nanocomposites at varied NiS contents are depicted in Fig. 7. The obtained results reveal that all the prepared samples harvest visible light. The values of the band gap

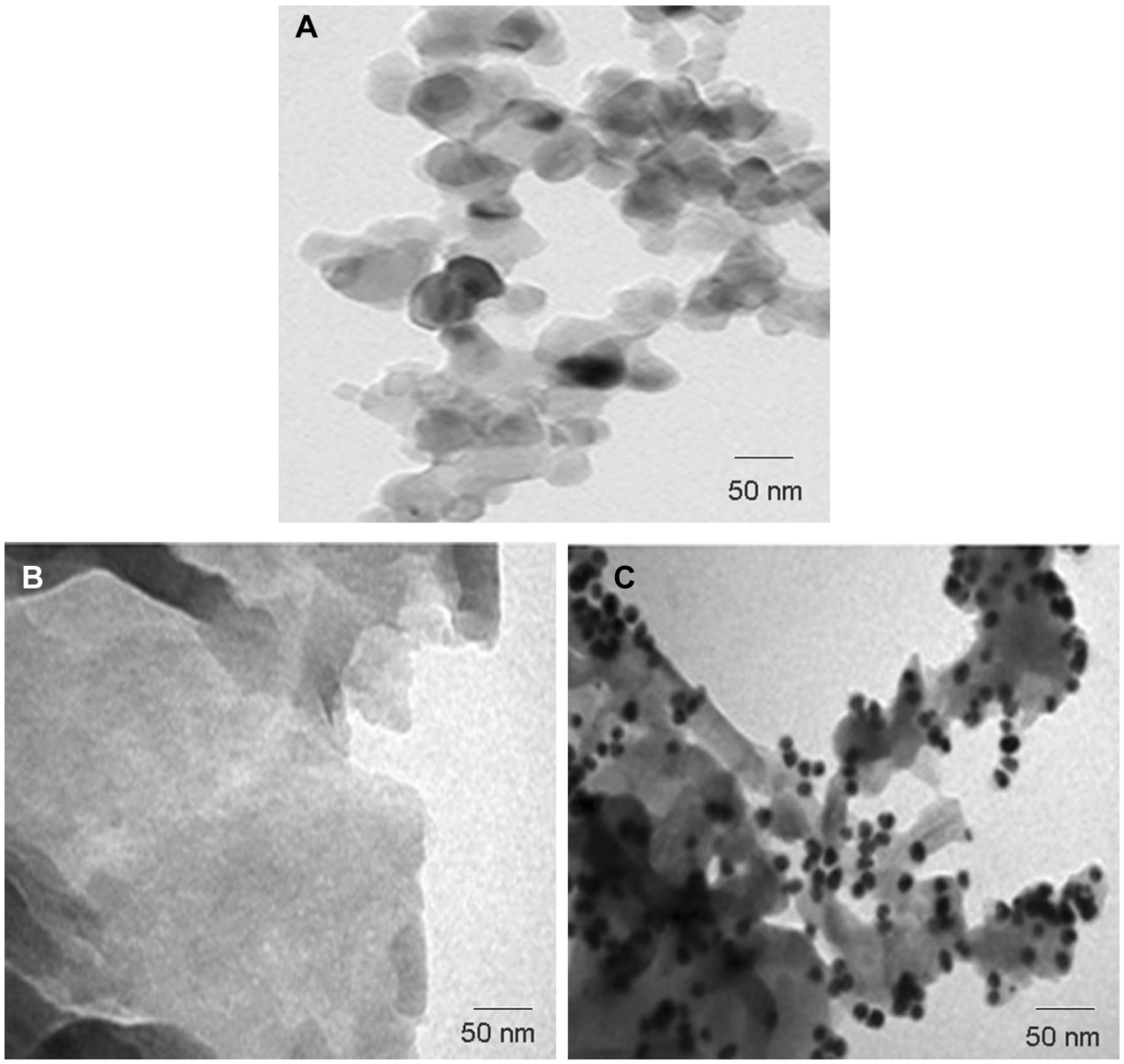

Fig. 4 TEM images for NiS (**a**), g-C_3N_4 (**b**) and 15 wt% NiS/pg-C_3N_4 nanocomposite (**c**) samples

determined from UV–Vis spectra and the data collected are shown in Table 1. The results indicated that NiS weight percentage is extremely significant in the obtained band gap values of pg-C_3N_4. In general, higher weight percent of incorporated NiS nanoparticle onto pg-C_3N_4 leads to lower value of the band gap of the produced nanocomposites.

Application of the H_2 evolution reaction

The prepared nanocomposite's photocatalysis has been performed and contrasted with pure NiS and g-g-C_3N_4 for evolution of hydrogen upon illumination applying visible light with maintaining the following reaction conditions: 500 W Xe lamp as light origin, 1.5 g/L photocatalyst loading, 450 mL volume of solution containing 10 vol% glycerol and 9 h illumination time at room temperature. Figure 8 shows the influence of NiS weight percent (5–20 wt%) /g-C_3N_4 nanosheets on hydrogen evolution quantity compared with pure NiS and g-C_3N_4. These findings reflected that hydrogen evolution quantity of pure g-C_3N_4 nanosheets and NiS nanoparticles is 210 and 500 µmol/g, respectively. The use of 5, 10, 15, and 20 wt% NiS/g-C_3N_4 photocatalysts in the photoreaction generates H_2 evolution of 11,000, 15,000, 24,000 and 24,500 µmol/g, respectively. This can be directly attributed to the decrease in the band gap values, large area, highly separation of charge carriers and can decrease the crystallite size of g-C_3N_4 nanosheets by addition of NiS nanoparticles. Increasing the photocatalyst loading of the 15 wt% NiS/g-C_3N_4 positively affects the yield of the reaction up to a certain loading after which the yield starts to decline with the increase of the amount of photocatalyst added to the reaction mixture. Figure 9 displayed that the hydrogen evolution boosted to 11,000, 15,000 and 24,000 µmol/g with the increase the photocatalyst loading 0.5–1.5 g/L, respectively.

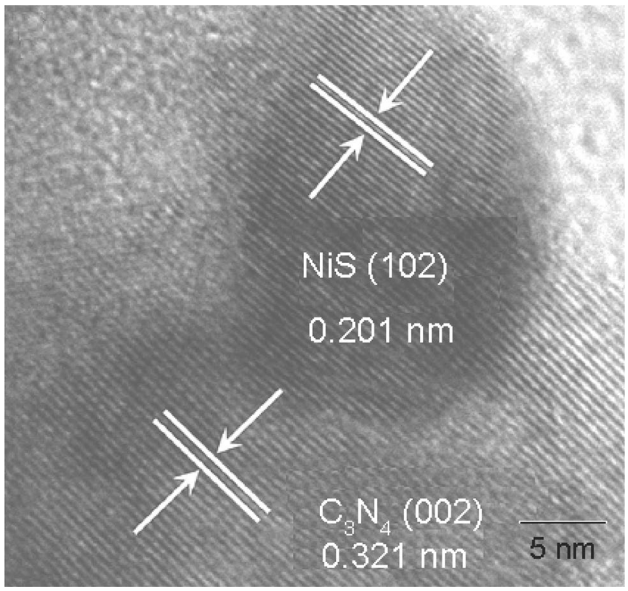

Fig. 5 HRTEM image for NiS@ pg-C_3N_4 nanocomposite sample

These results could be explained by increase in numerous active sites on the surface of 15% NiS/g-C_3N_4 photocatalyst. When the photocatalyst loading was boosted above 2.0 g/L, the hydrogen evaluation quantity declined to 14,000 µmol/g. This might be attributed to a reduction in penetration of light owing to high photocatalyst loading particles in suspension solution (see Table 2).

Our results were confirmed by conducting PL measurements and transient photocurrent responses. Pl spectra show that g-C_3N_4 has high-emission Pl intensity and the decoration of NiS nanoparticles onto g-C_3N_4 surface reduces the emission PL intensity (Fig. 10). PL emission intensities are ordered as follows: g-C_3N_4 > 5% NiS/g-C_3N_4 > 10% NiS/g-C_3N_4 > 15% NiS/g-C_3N_4 > 20% NiS/g-C_3N_4. Although NiS nanoparticles have low band gap value (2.17 eV), they have a high-emission PL intensity. Thus, the rate of the recombination of charge carriers in the case of NiS is very fast and NiS has low photocatalytic activity; however, incorporation renders an efficient photocatalyst as it is obvious in the photocatalytic activity

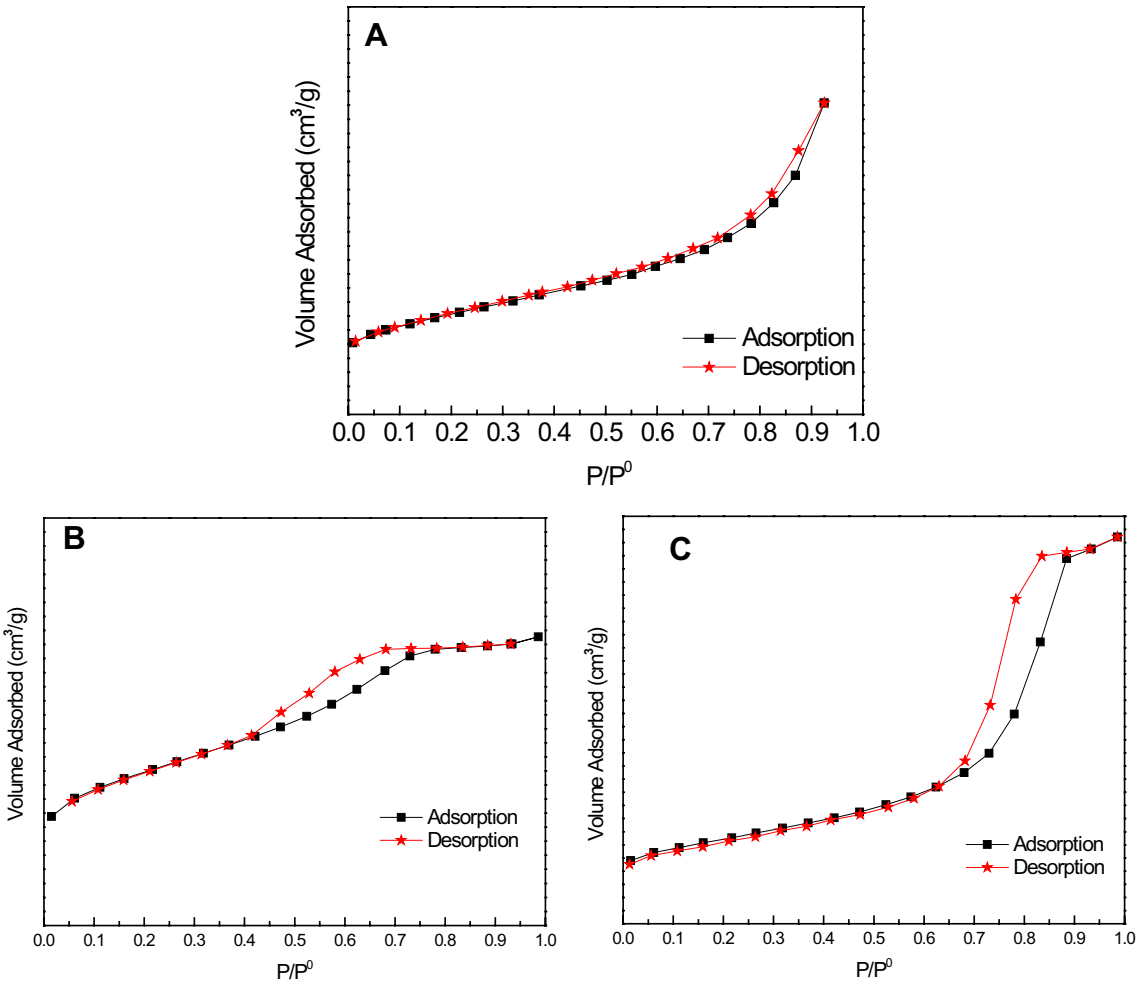

Fig. 6 N_2 adsorption–desorption isotherm of pure NiS (**a**), pg-C_3N_4 (**b**) and 15 wt% Ni/pg-C_3N_4 (**c**) nanocomposite

Table 1 BET surface area and band gap energy of pg-C_3N_4 and NiS@pg-C_3N_4 samples

Samples	$S_{BET,}$ (m^2/g)	Band gap (eV)
pg-C_3N_4	120 ± 2	2.67 ± 0.1
5 wt% NiS@pg-C_3N_4	110 ± 2	2.61 ± 0.1
10 wt% NiS@pg-C_3N_4	100 ± 2	2.53 ± 0.1
15 wt% NiS@pg-C_3N_4	90 ± 2	2.41 ± 0.1
20 wt% NiS@pg-C_3N_4	80 ± 2	2.21 ± 0.1
Pure NiS	30 ± 2	2.17 ± 0.1

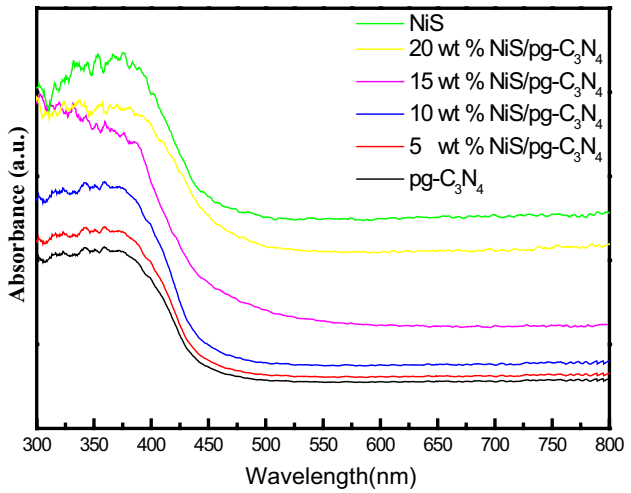

Fig. 7 UV–Vis spectra of NiS, pg-C_3N_4, and NiS/pg-C_3N_4 nanocomposites

Table 2 Comparison of photocatalytic activity of the present work on NiS@pg-C_3N_4 photocatalyst and previous published work

NiS wt% content	Hydrogen production (μmol/g/h)	References
0.76	16,400	Zhao et al. (2018)
1.5	44.77	Chen et al. (2014)
3.0	116. μmol g^{-1} h^{-1}	Chen et al. (2017)
5.0	29.68[1]	Hea et al. (2018)
15	24,000[1]	This work

section. Figure 11 shows transient photocurrent responses. g-C_3N_4 has low photocurrent density, but the deposition of NiS on its surface increases photocurrent density. Photocurrent density of the composites is arranged: g-C_3N_4 < 5 wt% NiS/g-C_3N_4 < 10 wt% NiS/g-C_3N_4 < 15 wt% NiS/g-C_3N_4 < 20 wt% NiS/g-C_3N_4. It is observed that the photocatalytic performance of the prepared nanocomposites is consistent and matched with PL measurements.

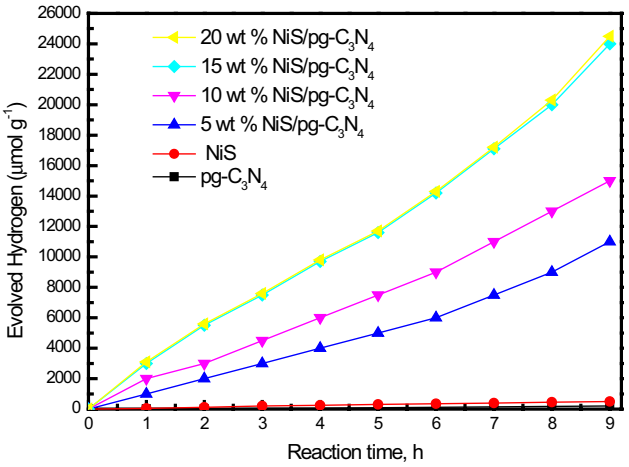

Fig. 8 Effect of wt% of NiS on amount of hydrogen evolution of NiS, pg-C_3N_4, and NiS/pg-C_3N_4 samples under the following reaction conditions: 500 W Xe lamp as light origin, 1.5 g/L photocatalyst loading, 450 mL volume of solution containing 10 vol% glycerol and 9 h illumination time at room temperature

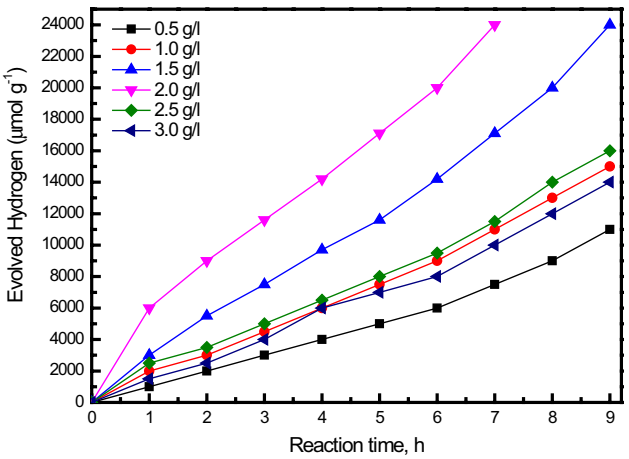

Fig. 9 Effect of 15% NiS/ pg-C_3N_4 photocatalyst on amount of hydrogen evolution under the following reaction conditions: 500 W Xe lamp as light origin, 450 mL volume of solution containing 10 vol% glycerol and 9 h illumination time at room temperature

Plausible mechanism of NiS/g-C_3N_4 nanocomposite

In an effort to explain hole–photoelectron separation between NiS nanoparticles and g-C_3N_4 nanosheets, the band energy levels could be calculated as in Table 3 as follows:

$$E_{CB} = X - 0.5\,E_g + E_0 \quad (1)$$

$$E_{VB} = E_g + E_{CB}, \quad (2)$$

where E_{VB} and E_{CB} are the valence and conduction bands, respectively, E_g is the band gap value collected from optical measurements, X is the absolute semiconductor

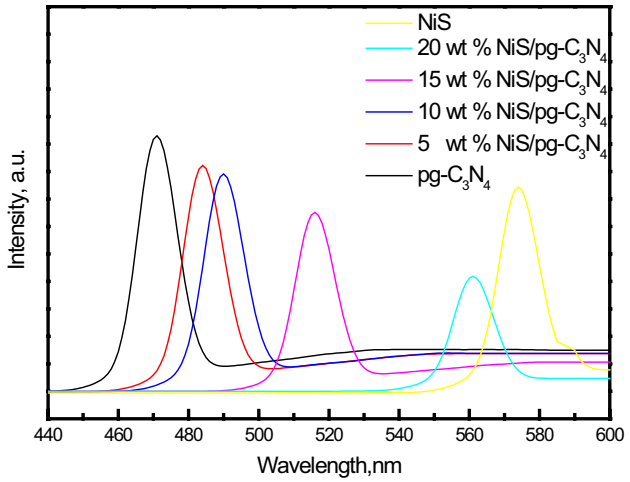

Fig. 10 Pl spectra of NiS, pg-C_3N_4, and NiS/pg-C_3N_4 nanocomposites

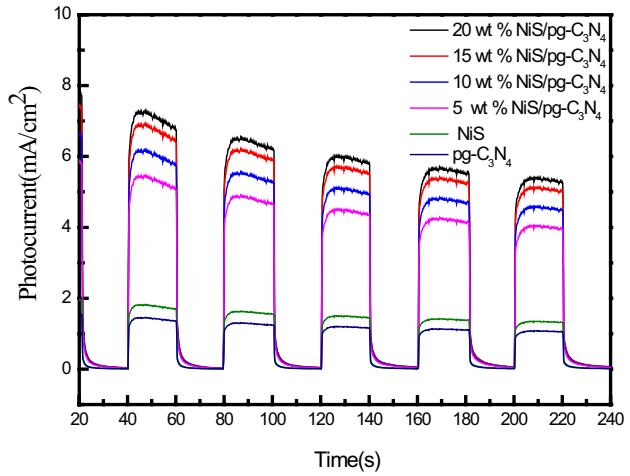

Fig. 11 Transient photocurrent responses of NiS, pg-C_3N_4, and NiS/pg-C_3N_4 nanocomposites

Table 3 The electronegativity, band gap, conduction band edge and valance band edge potential of the catalysts on normal hydrogen electrode

Semiconductor	χ, eV	E_g, eV	E_{CB}, ev	E_{VB}, ev
pg-C_3N_4	4.73	2.67	− 1.105	+1.565
Pure NiS	5.23	2.17	+0.296	+2.466

electronegativity and E_0 is a measuring the redox level versus normal hydrogen electrode to the absolute vacuum scale ($E_0 = -4.5$ eV).

As we stated earlier g-C_3N_4 has a narrow band gap value, thus could be easily excited by low energy. Upon illumination, pure g-C_3N_4 photogenerated electrons flow from

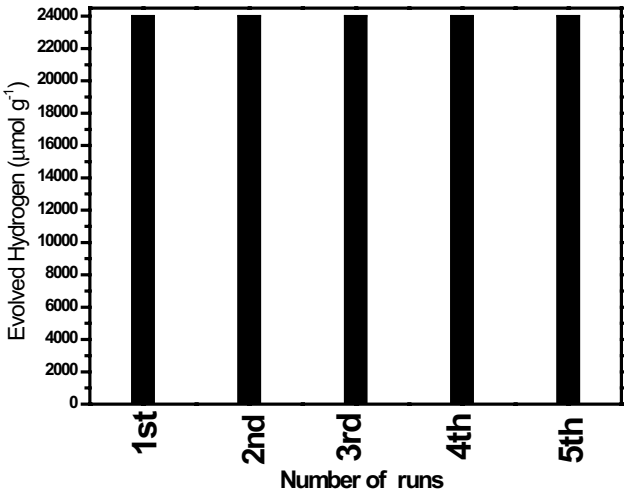

Fig. 12 Recycling and reuse of 15 wt% NiS/pg-C_3N_4 photocatalyst on amount of hydrogen evaluation under the following conditions: 500 W Xe lamp as light source, 2 g/L photocatalyst loading, 450 mL volume of solution containing 10 vol% glycerol and 7 h illumination time at room temperature

valance band to the conduction band. However, in case of NiS/g-C_3N_4 nanocomposite, the conduction band of NiS is more positive, hence NiS traps the excited electrons achieving the much desired charge carrier separation. Moreover, introducing NiS nanoparticles onto g-C_3N_4 nanosheets increases the numerous active sites on the surface of NiS/g-C_3N_4 photocatalyst and enhances the photocatalytic activity and accelerates the evolution of H_2. A third factor that increases the overall efficiency of the reaction is hole scavenging action by the presence of glycerol in the reaction solution; this process produces a proton that further reduces a recombination of charge carriers to generate H_2 again.

To explore the stability of the prepared photocatalyst, reuse and recycling of 15 wt % NiS/pg-C_3N_4 photocatalyst on hydrogen evaluation quantity was conducted under the following conditions: 500 W Xe lamp as light source, 2 g/L photocatalyst loading, 450 mL volume of solution containing 10 vol% glycerol and 7 h illumination time at room temperature. Figure 12 revealed that 15% NiS/pg-C_3N_4 photocatalyst is well stable and highly efficient without loss in the hydrogen production even after repeating five times.

Conclusions

g-C_3N_4 nanosheets were prepared by a facile combustion approach in presence of high mesoporous silica as a template. Subsequently, decoration of g-C_3N_4 nanosheet by NiS nanoparticles was performed by a hydrothermal process. Deposition of NiS on surface of g-C_3N_4 sheets decreases the band gap value of g-C_3N_4 sheets, hinders electron–hole

recombination. Highest amount of hydrogen evolution (24,000 μmol/g) was produced using 15 wt % NiS/g-C_3N_4 photocatalyst and 2.0 g photocatalyst loading for 7 h irradiation time at room temperature. The amount of evolved hydrogen using NiS/g-C_3N_4 is greater than pure NiS nanoparticles and g-C_3N_4 sheets, due to synergetic effect NiS and g-C_3N_4. NiS/g-C_3N_4 is well stable and highly efficient without loss in the hydrogen production even after repeating five times.

Acknowledgements This project was funded by the Deanship of Scientific Research (DSR) at King Abdulaziz University, Jeddah, under grant no. RG-18-130-38. The authors, therefore, acknowledge DSR for technical and financial support.

References

Anandan S, Wu JJ, Bahnemann D, Emelined A, Ashokkumar M (2017) Crumpled Cu_2O- g-C_3N_4 nanosheets for hydrogen evolution catalysis. Colloids Surf A 527:34–41

Bao Y, Chaen K (2017) A novel Z-scheme visible light driven Cu_2O/ Cu/ g-C_3N_4 photocatalyst using metallic copper as a charge transfer mediator. Mol Catal 432:187–195

Chen XB, Li C, Gratzel M, Kostecki R, Mao SS (2012) Nanomaterials for renewable energy production and storage. Chem Soc Rev 41:7909–7937

Chen Z, Sun P, Zhang B, Fan Z, Fang X (2014) In situ template-free ion-exchange process to prepare visible-light-active g-C_3N_4 /NiS hybrid photocatalysts with enhanced hydrogen evolution activity, J Phys Chem C 118:7801–7807

Chen YB, Qin ZX, Wang XX, Guo X, Guo LJ (2015) Noble-metal-free Cu_2S-modified photocatalysts for enhanced photocatalytic hydrogen production by forming nanoscale p–n junction structure. RSC Adv 5:18159–18166

Chen F, Yang H, Wang X, Yu H (2017) Facile synthesis and enhanced photocatalytic H_2-evolution performance of NiS_2-modified g-C_3N_4 photocatalysts. Chin J Catal 38:296–304

Cheng F, Yin H, Xiang Q (2017) Low-temperature solid-state preparation of ternary CdS/g-C_3N_4/CuS nanocomposites for enhanced visible-light photocatalytic H_2-production activity. Appl Surf Sci 391:432–439

Dong G, Zhang Y, Pan Q, Qiu J (2014) A fantastic graphitic carbon nitride (g-C_3N_4) material: electronic structure, photocatalytic and photoelectronic properties. J Photochem Photobiol C 20:33–50

Du Y, Huang Z, Wu S, Xiong K, Zhang X, Zheng B, Nadimicherla R, Fu R, Wu D (2018) Preparation of versatile yolk-shell nanoparticles with a precious metal yolk and a microporous polymer shell for high-performance catalysts and antibacterial agents. Polymer 137:195–200

Ganesh Babu S, Vinoth R, Surya Narayana P, Bahnemann D, Neppolian B (2015) Reduced graphene oxide wrapped Cu_2O supported on C_3N_4: an efficient visible light responsive semiconductor photocatalyst. APl Mater 3:104415 1–8.

Hafeez HY, Lakhera SK, Bellamkonda S, Rao GR, Shankar MV, Bahnemann DW, Neppolian B (2018) Construction of ternary hybrid layered reduced graphene oxide supported g-C_3N_4-TiO_2 nanocomposite and its photocatalytic hydrogen production activity. Int J Hydrogen Energy 43:3892–3904

Hea K, Xiea J, Li M, Li X (2018) In situ one-pot fabrication of g-C_3N_4 nanosheets/NiS cocatalyst heterojunction with intimate interfaces for efficient visible light photocatalytic H_2 generation. Appl Surf Sci 430:208–217

Hou Y, Li JY, Wen ZH, Cui SM, Yuan C, Chen JH (2014) N-doped graphene/porous g-C_3N_4 nanosheets supported layered-MoS_2 hybrid as robust anode materials for lithium-ion batteries. Nano Energy 8:157–164

Ismail A, Bahnemann DW (2014) Photochemical splitting of water for hydrogen production by molecular photocatalysis: A Review. Solar Energy Mater Solar Cells 128:85–101

Jin L, Yue D, Xu ZW, Liang G, Zhang Y, Zhang JF, Zhang X, Wang Z (2014) Fabrication, mechanical properties, and biocompatibility of reduced graphene oxide reinforced nanofiber mats. RSC Adv 4:35035–35041

Khan U, Alam W, Raza D, Bahnemann M, Muneer (2018) One-pot, self-assembled hydrothermal synthesis of 3D flower-like CuS/g-C_3N_4composite with enhanced photocatalytic activity under visible-light irradiation. J Phys Chem Solids 115:59–68

Kristl M, Dojer B, Gyergyek S, Kristl J (2017) Synthesis of nickel and cobalt sulfide nanoparticles using a low cost sonochemical method. Heliyon 3:e00273

Kumar S, Surendar T, Baruah A, Shanker V (2013) Synthesis of a novel and stable g-C_3N_4–Ag_3PO_4 hybrid nanocomposite photocatalyst and study of the photocatalytic activity under visible light irradiation. J Mater Chem A 1:5333–5340

Li X, Yu J, Low J, Fang Y, Xiao J, Chen X (2015) Engineering heterogeneous semiconductors for solar water splitting. J Mater Chem A 3:2485–2534

Lin X, Liang, Z, Lu H, Lou X, Zhang S, Liu B, Zheng R, Liu R, Fu, Wu D (2017) Mechanochemistry: a green, activation-free and top-down strategy to high-surface-area carbon materials. ACS Sustain Chem Eng 5(10):8535–8540

Liu L, Yuehong Qi J, Hu Y, Liang W, Cui (2015) Efficient visible-light photocatalytic hydrogen evolution and enhanced photostability of core@shell Cu_2O@ g-C_3N_4 octahedra. Appl Surf Sci 351:1146–1154

Liua L, Xua X, Si Z, Wanga Z, Rana R, He Y, Weng D (2018) Noble metal-free NiS/P-S codoped g-C_3N_4 photocatalysts with strong visible light absorbance and enhanced H_2 evolution activity. Catal Commun 106:55–59

Luo P, Zhang H, Liu L, Zhang Y, Deng J, Xu C, Hu N, Wang Y (2017) Targeted synthesis of unique nickel sulfides (NiS, NiS_2) microarchitectures, and the applications for the enhanced water splitting system. ACS Appl Mater Interfaces 9(3):2500–2508

Luo XL, He GL, Fang YP, Xu YH (2018) Nickel sulfide/graphitic carbon nitride/strontium titanate (NiS/ g-C_3N_4/$SrTiO_3$) composites with significantly enhanced photocatalytic hydrogen production activity. J Colloid Interface Sci 518:184–191

Mai W, Zuo Y, Li C, Wu J, Leng K, Zhang X, Liu R, Fu R, Wu D (2017) Functional nanonetwork-structured polymers with inbuilt poly(acrylic acid) linings for enhanced adsorption. Polym Chem 8(33):4771–4775

Meng X, Tian G, Chen Y, Zhai R, Zhou J, Shi Y, Cao X, Zhou W, Fu H (2013) Hierarchical CuS hollow nanospheres and their structure-enhanced visible light photocatalytic properties. Cryst Eng Comm 15:5144–5149

Misra M, Gupta RK, Paul AK, Singla M (2015) Influence of gold core concentration on visible photocatalytic activity of gold-zinc sulfide core-shell nanoparticle. J Power Sources 294:580–587

Misra M, Singh N, Gupta RK (2017) Enhanced visible-light-driven photocatalytic activity of Au@Ag core-shell bimetallic nanoparticles immobilized on electrospun TiO_2 nanofibers for degradation of organic compounds. Sci Technol 7:570–580

Mohamed RM, Aazam ES (2011) Characterization and catalytic properties of nano-sized au metal catalyst on titanium containing high mesoporous silica (Ti-HMS) synthesized by photo-assisted deposition and impregnation methods. Int J Photoenergy 2013:1–7

Mozaffari S, Tchoukov P, Mozaffari A, Atias J, Czarnecki J, Nazemifard N (2017a) Capillary driven flow in nanochannels—Application to heavy oilrheology studies. Colloids Surfaces A Physicochem Eng Aspects 513:178–187

Mozaffari S, Li W, Thompson C, Ivanov S, Seifert S, Lee B, Kovarik L, Karima AM (2017b) Colloidal nanoparticle size control: Experimental and kinetic modeling investigation of the ligand-metal binding role in controlling the nucleation and growth kinetics. Nanoscale 9:13772–13785

Peng S, Zhang S, Yang H, Wang H, Yu S, Zhang F, Peng (2014) Synthesis and characterization of g-C_3N_4/Cu_2O composite catalyst with enhanced photocatalytic activity under visible light irradiation. Mater Res Bull 56:19–24

Prakash J, Sun S, Swart HC, Gupta RK (2018) Noble metals-TiO_2 nanocomposites: from fundamental mechanisms to photocatalysis, surface enhanced Raman scattering and antibacterial applications. Appl Mater Today 11:82–135

Raza W, Bahnemann D, Muneer M (2017) Efficient visible light driven, mesoporous graphitic carbon nitrite based hybrid nanocomposite: with superior photocatalytic activity for degradation of organic pollutant in aqueous phase. J Photochem Photobiol A 342:102–115

Singh N, Mondal K, Misra M, Sharma A, Gupta RK (2016) Quantum dot sensitized electrospun mesoporous titanium dioxide hollow nanofibers for photocatalytic applications. RSC Adv 6:48109–48119

Singh N, Prakash J, Gupta RK (2017) Design, system, application statement. Mol Syst Des Eng 2:422–439

Tyagi KM, Tripathi N, Singh S, Choudhary, Gupt RK (2016) Green synthesis of carbon quantum dots from lemon peel waste: applications in sensing and photocatalysis. RSC Adv 6:72423–72432

Wang JC, Yao HC, Fan ZY, Zhang L, Wang JS, Zang SQ, Li ZJ (2016) Indirect Z-scheme BiOI/g-C_3N_4 photocatalysts with enhanced photoreduction CO_2 activity under visible light irradiation. ACS Appl Mater Interfaces 8:3765–3775

Wen J, Li X, Li H, Ma S, He K, Xu Y, Fang Y, Liu W, Gao Q (2015) Enhanced visible-light H_2 evolution of g-C_3N_4 photocatalysts via the synergetic effect of amorphous NiS and cheap metal-free carbon black nanoparticles as co-catalysts. Appl Surf Sci 358:204–212

Wen J, Xie J, Yang Z, Shen R, Li H, Luo X, Chen X, Li X (2017) Fabricating the robust g-C_3N_4 nanosheets/carbons/NiS multiple heterojunctions for enhanced photocatalytic H2 generation: An insight into the tri-functional roles of nanocarbons. ACS Sustain Chem Eng 5(3):2224–2236

Yang H, Jin Z, Hu H, Bi Y, Lu G (2018) Ni-Mo-S nanoparticles modified graphitic C_3N_4 for efficient hydrogen Evolution. Appl Surf Sci 427:587–597

Ye S, Wang R, Wu MZ, Yuan YP (2015) A review on g-C_3N_4 for photocatalytic water splitting and CO_2 reduction. Appl Surf Sci 358:15–27

Zhang J, Zhang M, Zhang G, Wang X (2012) Synthesis of carbon nitride semiconductors in sulfur flux for water photoredox catalysis. ACS Catal 2:940–948

Zhao H, Zhang H, Cui G, Dong Y, Wang G, Jiang P, Wu X, Zhao N (2018) A photochemical synthesis route to typical transition metal sulfides as highly efficient cocatalyst for hydrogen evolution: from the case of NiS/ g-C_3N_4. Appl Catal B 225:284–290